Turkish Journal of Physics

http://journals.tubitak.gov.tr/physics/

Research Article

Turk J Phys
(2020) 44: 57 – 66
© TÜBİTAK
doi:10.3906/fiz-1909-10

Structural and optical properties of ZnO films obtained on mesoporous Si substrates by the method of HF magnetron sputtering

Valeriy KIDALOV[1,*], **Alena DYADENCHUK**[2], **Yuriy BACHERIKOV**[3], **Anton ZHUK**[3], **Tetyana GORBANIUK**[3], **Igor ROGOZIN**[1], **Vitali KIDALOV**[1]

[1]Berdyansk State Pedagogical University, Berdyansk, Ukraine
[2]Dmytro Motornyi Tavria State Agrotechnological University, Melitopol, Ukraine
[3]V. Lashkaryov Institute of Semiconductor Physics, National Academy of Sciences of Ukraine, Kyiv, Ukraine

Received: 20.09.2019 • **Accepted/Published Online:** 28.01.2020 • **Final Version:** 12.02.2020

Abstract: In the present work, ZnO films were obtained on mesoporous silicon substrates by the method of HF magnetron sputtering of a metallic zinc target in reaction oxygen and argon gas medium. The properties of the ZnO films obtained on mesoporous substrates were studied depending on the ratio of the partial pressures of the working gases (argon/oxygen). X-ray analysis showed that in the process of deposition, the ZnO films of a hexagonal structure were formed. The effect of the porous layer on the structural and luminescent properties of the thin ZnO films was studied. The results showed that the porous silicon substrate reduces residual stresses and can be used for obtaining high-quality ZnO films.

Key words: ZnO film, porous Si, HF magnetron sputtering

1. Introduction

The interest in ZnO films as promising materials for various optoelectronic applications is currently growing [1–4]. The potential possibility of ZnO to replace gallium nitride attracts special interest towards thin films ZnO. ZnO-based structures surpass nitrides in thermal stability, and they are also resistant to chemical reactions and oxidation [5].

To obtain ZnO epitaxial films the substrates of gallium nitride [6] and silicon carbide [7] can be used. However, the high cost of these substrates prevents their widespread use for the production of ZnO films.

The ZnO/Si system has been actively studied in recent years, but the issue of crystal lattice inconsistency caused by the difference in the lattice parameters of the film and the substrate remains an unresolved problem. Recently, porous substrates have been used in heterostructures to reduce mechanical stresses.

We previously obtained single-crystal films of silicon carbide on mesoporous silicon substrates by the HVPE method (chemical substitution) [8]. The mechanical stresses of the structure were calculated experimentally and theoretically using the Comsol MultiPhysics software package. It was shown that mechanical stresses in the presence of a porous buffer layer are ~65 MPa and in the absence of a buffer layer they are ~125 MPa [9].

Thus, the porous structure reduces the contact area between the film and the substrate. This allows to effectively reduce the elastic stresses arising from the difference in thermal expansion coefficients and lattice parameters.

*Correspondence: kidalovv.v@gmail.com

This work is licensed under a Creative Commons Attribution 4.0 International License.

In this regard, a further study of the growth process of ZnO films on porous Si as well as the influence of the intermediate porous layer on elastic stresses in the ZnO/porous-Si/Si heterosystem seems to be relevant.

The purpose of this work is to study the properties of zinc oxide films obtained by the reactive HF magnetron sputtering method on mesoporous silicon substrates of orientation (100), depending on the ratio of partial pressures of the working gases (argon/oxygen).

2. Experimental technique

Samples of the porous silicon (Figure 1) obtained from Smart Membranes GmbH (Germany) were used as substrates. The parameters of the samples are shown in Table 1.

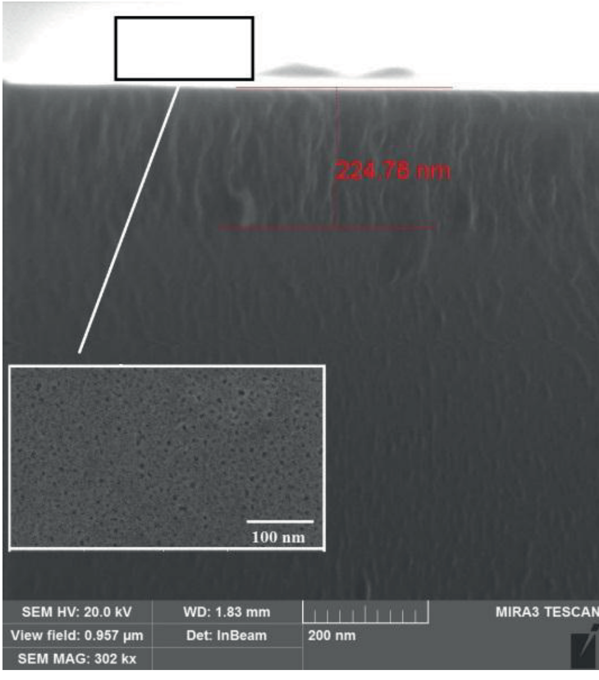

Figure 1. The SEM images of the Si (100) samples with the ensemble of mesopores.

The deposition of the ZnO thin films was carried out at an HF discharge power of 200 W in an argon medium with oxygen by sputtering a zinc target (80 mm in diameter and thickness of 6 mm). The zinc purity was 5 N. The distance between the target and substrate was 70 mm. The deposition time was 1200 s. The substrate temperature was fixed at 300 °C. Prior to the deposition, the target was presprayed for 10 min to remove all contaminants. Samples were divided into three groups depending on the conditions of the deposition process (Table 2).

Table 1. The parameters of porous-Si (100).

Parameter	Value
Depth of porous layer h, m	225 $\times 10^{-9}$
Pore diameter d, m	6.5 $\times 10^{-9}$
Wafer dimensions, m^2	10^{-4}

Table 2. The parameters of the deposition process of the thin ZnO films.

Parameter	Value		
	Sample 1	Sample 2	Sample 3
Residual pressure in the chamber, Pa	10^{-3}		
Argon pressure, Pa	1		
Oxygen pressure P_{O2}, Pa	0.05	0.1	0.5
Deposition time, seconds	1200		

All the experimental samples were studied using the following methods: scanning electron microscopy, AFM, X-ray diffraction, and photoluminescence. The structure of the interface and the surface structure of the ZnO layers on porous Si were studied using a scanning electron microscope (Tescan Mira 3 LMU), an energy dispersive spectrometer (Oxford Instruments X-Max 80 mm^2), an atomic force microscope, and an X-ray diffractometer (MiniFlex 600, Rigaku, Japan). The PL spectra with the temporal resolution were measured in the energy range of 1.4–3.2 eV with excitation by a nitrogen laser ($\lambda = 337$ nm, pulse duration of 8 ns) and stroboscopic registration of the signal in the photon-counting mode. The strobe width was 250 ns.

3. Results and discussion

The SEM images of the surface and cleaved facets of the obtained ZnO/porous-Si/Si samples demonstrate a significant change in the surface morphology of the porous silicon after synthesis.

On the surface of the samples, a structure of small (about tens to hundreds of nanometers) crystallites is observed. From the AFM images shown in Figure 2, it can be seen that for sample 3 (the maximum oxygen pressure) the densest ZnO nanostructures were obtained. These nanostructures contained grains the size of 100 nm and had the form of closely packed (agglomerated) nanograins (20–40 nm in size).

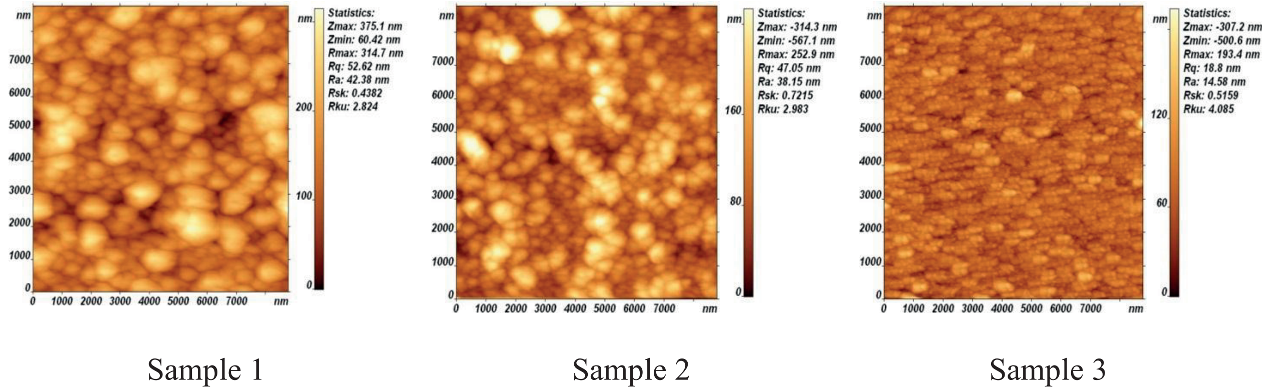

Figure 2. The AFM image of the surface of ZnO/porous-Si/Si heterostructures.

This was due to the fact that only at the highest O_2 stream the largest amount of oxygen inhibits crystallite growth and coalescence of ZnO. At the same time, new nucleation centers are created at the growth boundary in the presence of oxygen adatoms. This leads to the decrease in the size of crystallites and a change in the morphology of the samples.

The microelement analysis of the obtained surface is indicative of high stoichiometry of the ZnO film. The film thickness for all types of the samples is about 570–590 nm (Figure 3).

The ZnO film on all the samples is closely connected to the porous silicon substrate. No gap is observed on the film/substrate interface. This is probably due to the fact that ZnO particles penetrate the porous layer (Figure 3). The penetration of ZnO particles into the pores increases the adhesion of the film to the substrate and fixation of ZnO films in the PSi substrate.

However, as we showed in [10], an increase in annealing temperature leads to deterioration in the quality of ZnO film, which is due to the desorption of the film components.

Figure 4 shows a typical X-ray diffraction pattern of the ZnO films grown at a temperature of 300 °C on a PSi substrate. In the spectrum of the ZnO films, only the peak (002) is observed at 34.64°. This is characteristic of hexagonal type of ZnO. ZnO films have a predominant orientation along the c axis and a strong texture. The full width at half maximum (FWHM) of the peak (002) of the ZnO films is 0.73°.

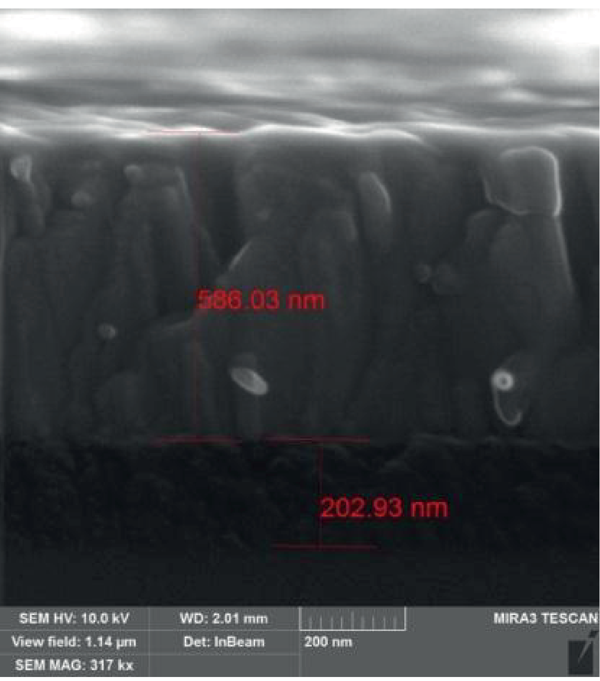

Figure 3. The SEM image of the cross-section of the ZnO/porous-Si/Si heterostructure.

The average crystallite size can be calculated from the position of the peak (002) by the Scherrer equation [11]:

$$D = \frac{b\lambda}{\beta \cos\theta},$$

where b is a correction factor of 0.94, λ is the X-ray wavelength, β is the FWHM of the peak (002) (in radians), and θ is the diffraction angle (in radians).

The lattice parameter c was calculated by the following equation: $\frac{1}{d^2} = \frac{4}{3}\left(\frac{h^2+hk+k^2}{a^2}\right) + \frac{l^2}{c^2}$ [11].

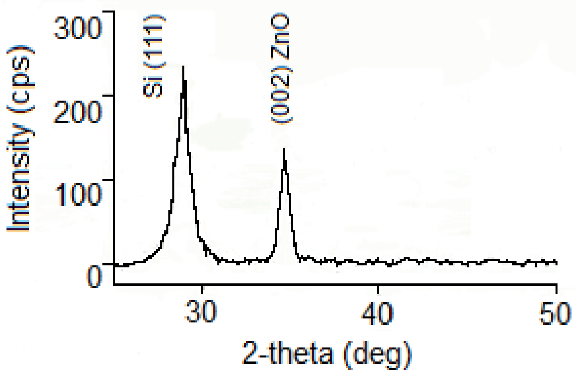

Figure 4. The X-ray diffraction pattern of the ZnO film grown on a PSi substrate with pores 500 nm in diameter.

The interplanar distance is calculated by the Wulff–Bragg formula: $2d_{hkl}\sin\theta = n\lambda$ [11]. The lattice parameter a can be calculated by the relation $\frac{c}{a} = \sqrt{\frac{8}{3}}$ [5].

The values of the average crystallite size D, interplanar distance d, and the c and a parameters of the crystal lattice are shown in Table 3.

Table 3. Structural properties of the ZnO films.

β, (°)	a, nm	c, nm	d, nm	L, nm	Grain size, nm (XRD)	Particle size, nm (SEM)	$\varepsilon\times10^{-3}$	$\delta\times10^{11}$ 1/nm^2	σ, GPa
0.73	3.1714	5.1788	0.258	0.194	11.92	200	2.61	0.0063	1.207

The XRD results showed that the synthesized ZnO films have a wurtzite structure with lattice parameters $a =$ 3.1714 nm and $c =$ 5.1788 nm. The calculated parameters are smaller than the real lattice parameters of the ZnO films (the lattice constants for the hexagonal ZnO film are given in the JCPDS data standard as $a_0 =$ 3.24982 nm and $c_0 =$ 5.20661 nm). The reason for this may be the fact that the structural properties of ZnO films are due to the porous structure of the silicon substrate.

The value of microstresses (ε) and the dislocation density (δ) can be calculated by the following expressions [12]: $\varepsilon = \left[\frac{\lambda}{D\cos\theta} - \beta\right] \times \frac{1}{\tan\theta}$ and $\delta = \frac{15\varepsilon}{Da}$.

The length L of the Zn – O bond is defined as [11]:

$$L = \sqrt{\left(\frac{a^2}{3} + \left(\frac{1}{2} - u\right)^2 c^2\right)},$$

where u is a displacement measure of an atom towards a neighboring one along the c axis. The value of u is calculated by the following formula: $u = a^2/3c^2 + 0.25$.

The value obtained for the length of bond L is shown in Table 3. It is known that the ionic radius of O^{2-} is 1.38 Å, and the ionic radius of Zn^{2+} is 0.83 Å [13]. Therefore, the length of the Zn – O bond is 2.21 Å. The value obtained for our samples corresponds perfectly well with the theoretical estimate of parameter L, which may indicate an insignificant content of structural defects (oxygen and zinc vacancies).

The difference in lattice constants and thermal expansion coefficients between Si and ZnO causes the appearance of residual stresses. The residual stress σ in the plane of the films can be calculated using the biaxial deformation model in the direction of the c axis [14]:

$$\sigma = \frac{2C_{13}^2 - C_{33}\left(C_{11} + C_{12}\right)}{2C_{13}} \times \frac{c - c_0}{c_0},$$

where C_{ij} are the elastic constants for ZnO ($C_{11} = 209.7$, $C_{12} = 121.1$, $C_{13} = 105.1$, $C_{33} = 210.9$ GPa [1]), and c and c_0 are the lattice parameters of the obtained ZnO film and ZnO film without deformation, respectively. If the stress is positive, then the biaxial stress is tensile; if the residual stress is negative, then the biaxial stress is compressional. The obtained value of deformation is 1.207 GPa. A positive value is connected with the tensile stress. A low value of the residual stress indicates a high quality of the obtained ZnO films.

As our studies show, the residual stresses of ZnO films grown on PSi are lower than those of films grown on Al_2O_3 [18] or Si [14,15]. Most researchers perform high-temperature annealing in the air or oxygen to reduce residual stresses [14–16].

Our ZnO films, obtained at a relatively "soft" temperature for synthesis conditions (300 °C), have a low value of residual stress and high crystalline perfection even without subsequent annealing. The comparison of our results with the results of other authors, for example [14,17], allows us to conclude that the low value of the residual stress is caused by the effect of a porous silicon substrate.

The calculated results for ZnO films obtained on PSi substrates are shown in Table 3.

Table 3 shows that there is a difference between the calculated value D and the observed particle size (according to the SEM data). Similar differences were observed by other authors [18]. In our opinion, the observed difference is due to the fact that not only the effect caused by spatial grain sizes but also microdeformations in the film as well as instrumental factors contribute to the broadening of the XRD reflections. Therefore, the real sizes of ZnO nanoparticles can be significantly larger than the values calculated by estimating the half-width of the peaks (002) in accordance with the Scherrer model. Thus, the results of the scanning electron microscopy and X-ray diffraction indicate high crystalline perfection of the obtained ZnO films.

The PL spectra at room temperature and liquid nitrogen of ZnO films obtained at various oxygen pressures P_{O2} are shown in Figure 5. The PL spectrum at room temperature of the obtained ZnO films shown in Figure 5a consists of a strong ultraviolet band centered at 382 nm (3.25 eV), and green and orange bands at 520 nm (2.38 eV) and 605 nm (2.05 eV), respectively. The spectral position of the peak at 382 nm (3.25 eV) is connected with the near-band-edge exciton emission in ZnO films. The radiation characteristics of various types of excitons in ZnO have been studied in detail [19,20].

As can be seen from the PL spectra of ZnO films grown at high pressures of P_{O2}, a sharp increase in the band of the exciton peak at 382 nm and a slight increase in the intensity of the bands in the visible region of the spectrum are observed. In contrast, a ZnO film grown at a minimum P_{O2} of 0.05 Pa exhibits a weak PL intensity, probably due to nonstoichiometric oxygen composition. The observed changes in the PL spectra are clearly correlated with AFM data. As can be seen from Figure 2, the quality of the films improves with increasing pressure of P_{O2}.

It was reported in [21,22] that the PL emission characteristics of ZnO films strongly depend on both the quality of the film and the stoichiometry of the film. Nevertheless, although the PL spectra of our samples show a clear correlation between the peak intensity of UV radiation and the quality of ZnO films, the green-orange emission is lower in a film with low crystallinity grown at a low pressure of P_{O2}. This observation may indicate

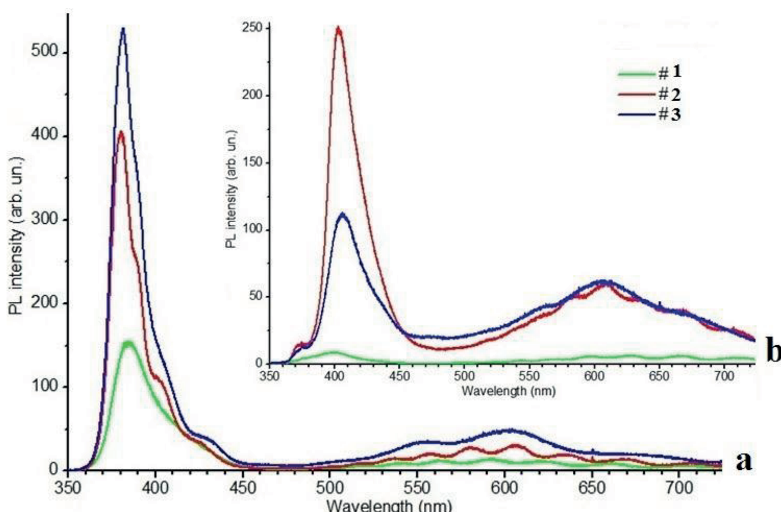

Figure 5. The PL of the ZnO films obtained on the surface of porous Si at a temperature of 300 K (a) and at 77 K (b).

that the emission properties of ZnO films are more dependent on stoichiometry than on the crystallinity of the film, since a ZnO film grown at a higher pressure of P_{O2} has improved stoichiometry with fewer oxygen vacancies and Zn interstices [22].

The radiation in the green region is usually connected with the defects in ZnO, such as oxygen vacancy (V_O), interstitial zinc (Zn_i), interstitial oxygen (O_i), and antisite defect (O_{Zn}) [23]. As shown by the authors of [23,24], in ZnO the orange band is localized at 636 nm (1.95 eV) and is associated with shallow donor-deep acceptor transitions, which have an energy level of about 0.5–0.6 eV above the valence band [23]. Obviously, the 605 nm (2.05 eV) band observed in our samples is associated with a porous silicon substrate. This is in good agreement with the results of [25], where the authors observed the 605 nm band in the PL spectra of porous silicon.

The low-temperature PL measurement was performed for a more detailed study of the radiation characteristics. Figure 5b shows the PL spectra obtained at 77 K from the same films as in Figure 5a. ZnO films grown in the pressure range of P_{O2} 0.1–0.5 Pa show an intense peak at 402 nm (~3.09 eV), as well as a weak emission peak associated with the exciton at 370.2 nm (~3.35 eV) and radiation associated with deep levels in the visible areas with a similar tendency at room temperature. As can be seen from Figure 5b, the exciton band is not observed in the PL spectrum of films grown at a minimum oxygen pressure, which can also be associated with nonstoichiometry of ZnO films.

Earlier, we showed in [26] that the band at 370.2 nm in ZnO is caused by the recombination of excitons at the neutral acceptor of zinc vacancy, and 402 nm is associated with radiative transitions in the conduction band or the acceptor, where there is intrinsic defect of the zinc vacancy V_{Zn} with a depth of ~0.3 eV above the ceiling of the valence band. We also showed in [27] that the concentration of zinc vacancies, depending on the conditions of heat treatment, can be 10^{17} to 10^{19} cm^{-3}. This is supported by the data of [28], wherein the authors also associated the observed band of 401 nm with a zinc vacancy. Recent theoretical calculations of the energy levels of intrinsic defects in ZnO give values of the depth of the zinc vacancy level of approximately 0.2–0.3 eV above the top of the valence band [29,30]. For example, according to the calculation in [29], for the energy interval from the bottom of the conduction band to the Zn (V_{Zn}) vacancy, the level of ~3.06 eV is in

good agreement with the energy of ~3.09 eV of violet radiation at 402 nm in this work. Therefore, the emission peak at 402 nm observed in this work should be attributed to the electron transition from the bottom of the conduction band to the Zn vacancy level. The nature of the green band at 520 nm (2.38 eV) will be investigated in the future.

The ratio of the ultraviolet radiation intensity to the intensity of the visible radiation is considered as the main criterion for assessing the quality of crystallinity. Thus, strong ultraviolet radiation and weak green radiation from ZnO can be explained by good crystalline quality of the ZnO film.

Thus, the observed photoluminescence spectra represent a combination of the radiation of the ZnO film (green and ultraviolet bands) and the porous silicon substrate (a red band). Obviously, by combining the radiation from a porous silicon substrate and a ZnO film, it is possible to obtain the resulting white luminescence. However, further research is required.

4. Conclusion

ZnO films on the surface of mesoporous silicon of orientation (100) were obtained by the method of HF magnetron sputtering. The properties of the three types of samples of the ZnO/porous-Si/Si heterostructure were studied, depending on the conditions of the deposition process. From the AFM images it can be seen that at the highest ratio of O_2 stream to argon stream, the densest ZnO nanostructures with the highest porosity were obtained. They contained well recognizable grains the size of 100 nm and had the form of closely packed (agglomerated) nanograins (20–40 nm in size). According to the XRD measurements, the ZnO films are oriented lengthwise (002) on the surface in both cases with an FWHM of the peak (002) of 0.73°. The ZnO films have a low value of residual compressive stress (1.207 GPa). The visible luminescence band is a combination of the green band of the ZnO film and the red band from the porous silicon substrate. With the temperature drop from 300 to 77 K, the PL band shifts to the long wavelength side and decrease in intensity. At the same time, the relative intensity of the bound exciton increases, the band of which becomes dominant in the PL spectrum.

References

[1] Fan JC, Sreekanth KM, Xie Z, Chang SL, Rao KV. p-Type ZnO materials: Theory, growth, properties and devices. Progress in Materials Science 2013; 58: 874. doi: 10.1016/j.pmatsci.2013.03.002

[2] Ye ZZ, Lu JG, Zhang YZ, Zeng YJ, Chen LL et al. ZnO light-emitting diodes fabricated on Si substrates with homobuffer layers. Applied Physics Letters 2007; 91: 113503. https://doi.org/10.1063/1.2783262

[3] Hsiao C, Huang S, Chang R. Temperature field analysis for ZnO thin-film pyroelectric devices with partially covered electrode. Sensors and Materials 2012; 24: 421-441. doi: 10.18494/SAM.2012.782

[4] Sathya M, Claude A, Govindasamy P, Sudha K. Growth of pure and doped ZnO thin films for solar cell applications. Advances in Applied Science Research 2012; 3 (5): 2591-2598.

[5] Morkoç H, Özgür Ü. Thin Oxide: Fundamentals, Materials and Device Technology. Berlin, Germany: Wiley-VCH, 2009.

[6] Oh DC, Suzuki T, Makino H, Hanada T, Ko HJ et al. Electrical properties of ZnO/GaN heterostructures and photo-responsivity of ZnO layers. Physica Status Solidi (C) 2006; 3 (4): 946-951. doi: 10.1002/pssc.200564758

[7] Kukushkin SA, Osipov AV, Romanychev AI. Epitaxial growth of zinc oxide by the method of atomic layer deposition on SiC/Si substrates. Physics of the Solid State 2016; 58 (7): 1448-1452. doi: 10.1134/S1063783416070246

[8] Kidalov VV, Kukushkin SA, Osipov AV, Redkov AV, Grashchenko AS et al. Properties of SiC films obtained by the method of substitution of atoms on porous silicon. ECS Journal of Solid State Science and Technology 2018; 7 (4): P1-P3. doi: 10.1149/2.0061804jss

[9] Kidalov VV, Kukushkin SA, Osipov AV, Redkov AV, Grashchenko AS et al. Growth of SiC films by the method of substitution of atoms on porous Si (100) and (111) substrates. Materials Physics and Mechanics 2018; 36: 39-52. doi: 10.18720/MPM.3612018_4

[10] Rogozin IV, Georgobiani AN, Kotlyarevsky MB, Demin VI, Lepnev LS. Activation of p-type conduction in ZnO: N films by annealing in atomic oxygen. Inorganic Materials 2013; 49: 568-571. doi: 10.1134/S0020168513050130

[11] Singh A, Vishwakarma HL. Study of structural, morphological, optical and electroluminescent properties of undoped ZnO nanorods grown by a simple chemical precipitation. Materials Science-Poland 2015; 33: 751-759. doi: 10.1515/msp-2015-0112

[12] Rogozin IV, Kotlyarevsky MB. Characteristics of nitrogen-doped p-ZnO thin films and ZnO/ZnSe p–n heterojunctions grown on a ZnSe substrate. Semiconductor Science and Technology 2008; 23: 085008. doi: 10.1088/0268-1242/23/8/085008

[13] Fan JC, Sreekanth KM, Xie Z, Chang SL, Rao KV. p-Type ZnO materials: Theory, growth, properties and devices. Progress in Materials Science 2013; 58: 874. doi: 10.1016/j.pmatsci.2013.03.002

[14] Kim MS, Yim KG, Leem JY, Kim S, Nam G et al. Thickness dependence of properties of ZnO thin films on porous silicon grown by plasma-assisted molecular beam epitaxy. Journal of the Korean Physical Society 2011; 59: 2354-2361. doi: 10.3938/jkps.59.2354

[15] Ozen I, Gulgun MA. Residual stress relaxation and microstructure in ZnO Thin Films. Advances in Science and Technology 2006; 45: 1316-1321. doi: 10.4028/www.scientific.net/AST.45.1316

[16] Ting SY, Chen PJ, Wang HC, Liao CH, Chang WM et al. Crystallinity improvement of ZnO thin film on different buffer layers grown by MBE. Journal of Nanomaterials 2012; 17: 929278. doi: 10.1155/2012/929278

[17] Cai H, Shen H, Yin Y, Lu L, Shen J et al. The effects of porous silicon on the crystalline properties of ZnO thin films. Journal of Physics and Chemistry of Solids 2009; 70: 967-971. doi: 10.1016/j.jpcs.2009.05.004

[18] Patil AV, Dighavkar CG, Sonawane SK, Shinde UP, Patil SJ et al. Study of microstructural parameters of screen printed ZnO thick film sensors. Sensors & Transducers Journal 2010; 117: 62-70.

[19] Wagner MR, Callsen G, Reparaz JS, Schulze JH, Kirste R et al. Bound excitons in ZnO: Structural defect complexes versus shallow impurity centers. Physical Review B 2011; 84: 035313. doi.org/10.1103/PhysRevB.84.035313

[20] Meyer BK, Sann J, Lautenschläger S, Wagner MR, Hoffmann A. Ionized and neutral donor-bound excitons in ZnO. Physical Review B 2007; 76: 184120. doi.org/10.1103/PhysRevB.76.184120

[21] Tang ZK, Wong GKL, Yu P. Room-temperature ultraviolet laser emission from self-assembled ZnO microcrystallite thin films. Applied Physics Letters 1998; 72: 3270. doi: 10.1063/1.121620

[22] Vanheusden K, Seager CH, Warren WL, Tallant DR, Voigt JA. Correlation between photoluminescence and oxygen vacancies in ZnO phosphors. Applied Physics Letters 1996; 68: 403-405. doi: 10.1063/1.116699

[23] Reshchikov MA, Morkoc H, Nemeth B, Nause J, Xie J et al. Luminescence properties of defects in ZnO. Physica B: Condensed Matter 2007; 401-402: 358-361. doi: 10.1016/j.physb.2007.08.187

[24] Reshchikov MA, Xie JQ, Hertog B, Osinsky A. Yellow luminescence in ZnO layers grown on sapphire. Journal of Applied Physics 2008; 103: 103514. doi: 10.1063/1.2924437

[25] Göring P, Lelonek M. Highly ordered porous materials. In: Van de Voorde M (editor). Nanoscience and Nanotechnology: Advances and Developments in Nano-sized Materials. Berlin, Germany: De Gruyter, 2018, pp. 208-233.

[26] Georgobiani AN, Kotlyarevskii MB, Kidalov VV, Lepnev LS, Rogozin IV. Luminescence of native-defect p-type ZnO. Inorganic Materials 2001; 37: 1095-1098. doi: 10.1023/A:1012581221305

[27] Rogozin IV, Marakhovskii AV. Intrinsic defects in ZnO and GaN crystals. Journal of Applied Spectroscopy 2005; 72: 833-839. doi: 10.1007/s10812-006-0012-5

[28] Jeong SH, Kim BS, Lee BT. Photoluminescence dependence of ZnO films grown on Si (100) by radio-frequency magnetron sputtering on the growth ambient. Applied Physics Letters 2003; 82: 2625-2627. doi: 10.1063/1.1568543

[29] Zhao S, Zhou Y, Zhao K, Liu Z, Han P et al. Violet luminescence emitted from Ag-nanocluster doped ZnO thin films grown on fused quartz substrates by pulsed laser deposition. Physica B: Condensed Matter 2006; 373: 154-156. doi: 10.1016/j.physb.2005.11.116

[30] Hu J, Pan BC. Electronic structures of defects in ZnO: Hybrid density functional studies. Journal of Chemical Physics 2008; 129: 154706. doi: 10.1063/1.2993166